technologies

MDPI

Article

Multi-Timescale Cooperative Voltage Control Method for New Power Systems Under Sandstorm Weather

Qian Zhang [1], Lu Liu [2], Huiping Zheng [1], Xueting Cheng [1], Juan Wei [2,*], Ji Zhang [2] and Yuxiang Li [2]

[1] State Grid Shanxi Electric Power Research Institute, Taiyuan 030001, China; qianzhang@whu.edu.cn (Q.Z.); zhenghuiping@sx.sgcc.com.cn (H.Z.); chengxueting@sx.sgcc.com.cn (X.C.)
[2] College of Electrical and Information Engineering, Hunan University, Changsha 410082, China; lls2024@hnu.edu.cn (L.L.); jizhang@hnu.edu.cn (J.Z.); l2447393130@hnu.edu.cn (Y.L.)
* Correspondence: weijuanba@hnu.edu.cn

Abstract

To address the challenges of rapid voltage fluctuations and operational economy in new power systems with high wind power integration under sandstorm weather, this paper proposes a multi-timescale cooperative voltage control strategy for new power systems. On the second-level timescale, a discrete state-space model of wind turbines and reactive power devices is established considering sudden wind speed changes. Model predictive control (MPC) is then used to rapidly calculate the optimal reactive power references for wind turbines, static var generator (SVG), and on-load tap changer (OLTC), thereby effectively ensuring rapid stabilization of the grid-connection point voltage. On the minute-level timescale, a two-stage topology reconfiguration method is adopted. A feasible radial network is first generated through a sequential switch opening strategy, followed by iterative optimization via a switch exchange strategy. This approach rapidly identifies the optimal switch configuration to minimize network losses and improve operational economy. Simulation results demonstrate the effectiveness of the proposed strategy in voltage regulation and loss reduction, highlighting its capability to enhance the robustness of new power systems under sandstorm weather.

Keywords: new power system; voltage control; sandstorm weather; optimal control

1. Introduction

With the rapid growth of wind power integration, clean energy utilization has been greatly enhanced [1]. However, the increasing scale and complexity impose stricter requirements on real-time computation and grid control [2]. These challenges are especially pronounced under extreme weather such as sandstorms. The drastic wind speed variations induced by sandstorms cause severe fluctuations in wind turbine output power, leading to rapid and frequent voltage fluctuations that threaten second-level voltage stability [3]. Meanwhile, the growing scale of new power systems makes traditional centralized optimization methods suffer from high computational complexity, as they cannot meet the real-time requirements of online applications, thus failing to achieve both voltage security and minute-level economic optimization [4]. Therefore, developing a cooperative control framework to achieve fast voltage stabilization and economic optimization under sandstorm weather is a critical challenge.

Existing voltage control methods include centralized and distributed approaches. Centralized voltage control relies on a central controller to send commands to all regulation

Check for updates

Academic Editor: Julio Cesar Rosas Caro

Received: 29 July 2026
Revised: 5 September 2026
Accepted: 7 September 2026
Published: 7 September 2026

Copyright: © 2026 by the authors. Licensee MDPI, Basel, Switzerland. This article is an open access article distributed under the terms and conditions of the Creative Commons Attribution (CC BY) license.

devices [5]. For example, centralized model predictive control (MPC) is employed for global reactive power and voltage optimization, but it suffers from high communication dependency and computational delays [6]. To improve efficiency, distributed control uses multiple local controllers based on neighboring information [7]. The alternating direction method of multipliers (ADMM) is applied for distributed reactive power optimization of photovoltaic inverters, but it does not fully coordinate multiple types of reactive power devices [8]. A gradient projection-based method is developed to coordinate control of wind farms with on-load tap changer (OLTC) and static synchronous compensator, but it neglects the instantaneous impacts of sandstorm-induced wind speed variations and the mechanical delays of OLTCs [9]. Thus, these methods are inadequate for the fast voltage regulation required during sandstorms.

Network reconfiguration (NR) adjusts switch statuses to alter network topology, which reduces losses and improves voltage quality without additional hardware [10,11]. NR is formulated as a mixed-integer nonlinear programming problem. Existing solutions include mathematical programming (MP) and heuristic algorithms [12]. A mixed-integer linear programming (MILP) model is constructed for AC/DC hybrid network reconfiguration [13], while mixed-integer second-order cone programming (MISOCP) with observability constraints is employed for security enhancement [14]. However, these methods are computationally slow for large-scale systems and rely on accurate models. Heuristic methods based on probabilistic analysis and genetic algorithms have been proposed for intra-day reconfiguration, but they are conservative and time-consuming [15]. These approaches cannot meet the minute-level reconfiguration speed requirements under sandstorm weather.

Given the high penetration of renewables, single-timescale control strategies are insufficient [16,17]. Multi-timescale cooperative control has emerged as a promising solution [18,19]. A dual-timescale distributed voltage control framework using MPC and ADMM is developed to coordinate slow and fast devices, reducing losses and switching operations [20]. A distributionally robust chance-constrained MPC method is proposed for coordinated voltage control under high photovoltaic penetration [21]. Meanwhile, a dual-timescale voltage control method based on deep reinforcement learning is proposed to achieve both fast voltage regulation and long-term economy [22]. However, these methods mainly focus on renewable energy uncertainties under conventional operating conditions and lack sufficient consideration of extreme weather scenarios such as sandstorms. Under sandstorm conditions, wind speed exhibits high turbulence intensity, sharp fluctuations, and strong non-stationarity, resulting in rapid variations in wind turbine output power and severe voltage deviations. Moreover, the different dynamic response characteristics of wind turbine converters, SVG, and OLTC make coordinated control more challenging.

Therefore, the core challenge that sandstorm weather poses to voltage control is developing a control strategy that simultaneously meets the requirements of second-level response speed, disturbance robustness, and multi-device coordination. This constitutes the fundamental motivation for the multi-timescale cooperative control proposed in this paper. The main contributions of this paper are summarized as follows:

(1) A sandstorm-oriented multi-timescale cooperative voltage control framework is proposed for new power systems with high wind power penetration. The framework coordinates fast voltage regulation and slow economic optimization through the cooperation between second-level device control and minute-level network reconfiguration.
(2) An MPC-based coordinated voltage control method is developed to address rapid voltage fluctuations caused by sudden wind speed variations under sandstorm conditions. Unlike independent control of individual devices, the proposed method jointly optimizes wind turbine converters, SVG, and OLTC while considering their different dynamic response characteristics.

(3) A two-stage fast topology reconfiguration method is proposed to improve the computational efficiency of minute-level network optimization. The proposed strategy generates feasible radial configurations through sequential switch opening and further reduces losses through sensitivity-based switch exchange, making it suitable for online operation under extreme weather conditions.

The subsequent chapters of this paper are organized as follows. Section 2 introduces the multi-timescale voltage control framework. Section 3 details the wind farm voltage optimization control under sandstorm weather. Section 4 presents the two-stage topology reconfiguration method. Section 5 discusses the simulation results. Section 6 presents the conclusions.

2. Multi-Timescale Voltage Control Framework

A fast multi-timescale cooperative control and optimization strategy is proposed for new power systems with high renewable penetration under sandstorm weather, as shown in Figure 1. The strategy addresses voltage stability and economic optimization through second-level and minute-level coordination.

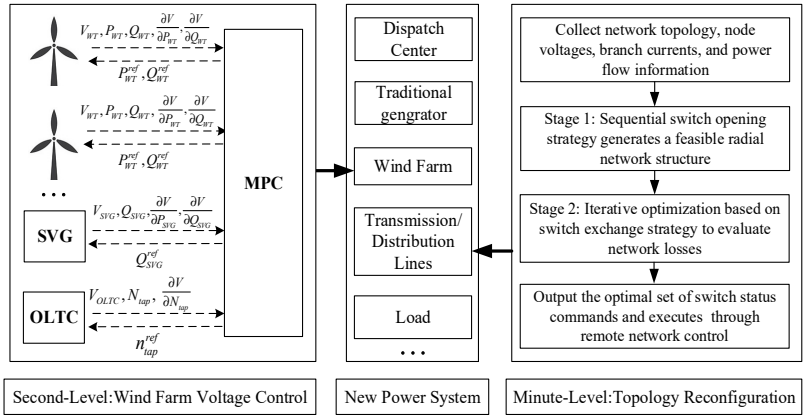


Figure 1. Multi-timescale cooperative voltage control block diagram for new power systems under sandstorm weather.

On the second-level timescale, an MPC controller is deployed in the wind farm. It collects real-time measurements including terminal voltages, active and reactive power outputs, rotor speeds of wind turbines, reactive power output of static var generator (SVG), and the OLTC tap position. Based on these data and pre-calculated voltage sensitivities, the MPC solves a finite-horizon optimization problem to generate the optimal reactive power references for each wind turbine, SVG and OLTC. This coordinated action ensures fast stabilization of the grid-connection point voltage. Meanwhile, the second-level MPC layer transmits the wind farm's operational state information to the minute-level topology reconfiguration layer at each control cycle. On the minute-level timescale, a centralized reconfiguration controller is deployed across the entire power network. It periodically collects system-wide data, including topology status, node voltages, branch currents, and power flows. The two-stage strategy generates a feasible radial network via sequential switch opening, reduces losses through iterative switch exchanges, and finally outputs the optimal switch status commands for execution through remote control units. This process efficiently solves the reconfiguration problem, reducing losses and improving economic operation.

3. Voltage Optimization Control of Wind Farms Under Sandstorm Weather

3.1. Modeling of Wind Turbines and Reactive Power Devices

The wind turbine model considers mechanical power capture, electrical response, and wind speed variations. The motion equation of wind turbines can be expressed as:

$$\frac{\mathrm{d}\omega}{\mathrm{d}t} = \frac{P_m - P}{2H_\mathrm{t}\omega} \tag{1}$$

where P_m is the mechanical power, P is the active power, ω is the rotor speed, and H_t is the inertia constant.

Performing Taylor expansion at the initial operating point (ω_0, P^0), the rotor speed variation of the wind turbine is expressed as:

$$\Delta\dot{\omega} = \frac{P^0 - P_\mathrm{m}}{2H_\mathrm{t}(\omega_0)^2}\Delta\omega - \frac{\Delta P}{2H_\mathrm{t}\omega_0} + \frac{K_v}{2H_\mathrm{t}\omega_0}\Delta v \tag{2}$$

where v is the wind speed, and K_v is the sensitivity coefficient of mechanical power to wind speed, and ΔP represents the variation of wind turbine active power output. According to the adopted power balance convention, an increase in electrical power output reduces the accelerating power of the rotor, which has a negative effect on rotor speed variation. Considering the dynamic response and time delay characteristics of the power converter, the active and reactive power control loops of the wind turbine are modeled as first-order inertia links:

$$\Delta P = \frac{1}{1 + sT_\mathrm{P}}\Delta P^\mathrm{ref} \tag{3}$$

$$\Delta Q = \frac{1}{1 + sT_\mathrm{Q}}\Delta Q^\mathrm{ref} \tag{4}$$

where T_P, T_Q are the time constants of the active power and reactive power control loops, and $\Delta P^{ref}, \Delta Q^{ref}$ are the active and reactive reference increment. Under sandstorm conditions, drastic wind speed variations directly change the mechanical power, thereby affecting the active power output. Therefore, the time-domain differential equation of active power is expressed as:

$$T_\mathrm{P}\frac{d\Delta P}{dt} + \Delta P = \Delta P^{ref} + K_v\Delta v \tag{5}$$

In this model, ΔP represents the dynamic variation of wind turbine active power output caused by wind speed disturbances and control commands. This active power variation is considered in the rotor dynamic model and voltage control process, establishing the relationship between wind disturbance, turbine output response, and voltage variation.

Furthermore, the partial derivatives of the power increments with respect to time are organized as:

$$\frac{d\Delta P}{dt} = -\frac{1}{T_\mathrm{P}}\Delta P + \frac{1}{T_\mathrm{P}}\Delta P^{ref} + \frac{K_v}{T_\mathrm{P}}\Delta v \tag{6}$$

$$\frac{d\Delta Q}{dt} = -\frac{1}{T_Q}\Delta Q + \frac{1}{T_Q}\Delta Q^{ref} \tag{7}$$

The increments of voltage magnitude are obtained using sensitivity coefficients:

$$\Delta V = \frac{\partial V}{\partial P}\Delta P + \frac{\partial V}{\partial Q}\Delta Q \tag{8}$$

where $\partial V/\partial P$, $\partial V/\partial Q$ represent the voltage magnitude sensitivity coefficients with respect to active and reactive power injections, respectively. The power variables follow the injection convention, where positive power variations indicate increased power injection

into the network. The voltage magnitude sensitivity coefficients with respect to active and reactive power injections are calculated by linearizing the AC power flow equations around the current operating point:

$$\frac{\partial V}{\partial P} = \frac{1}{\partial V}\mathrm{Re}\left(\underline{V}\frac{\overline{V}}{\partial P}\right), \frac{\partial V}{\partial Q} = \frac{1}{\partial V}\mathrm{Re}\left(\underline{V}\frac{\overline{V}}{\partial Q}\right) \tag{9}$$

The discrete state-space model of the wind turbine considering sandstorm weather conditions is constructed as:

$$\Delta x(k+1) = A\Delta x(k) + B\Delta u(k), \Delta y(k+1) = C\Delta x(k+1) \tag{10}$$

where $\Delta x(k+1) = [\Delta\omega(k+1), \Delta P(k+1), \Delta Q(k+1)]^T, \Delta x(k) = [\Delta\omega(k), \Delta P(k), \Delta Q(k)]^T$, $A = e^{A_d \Delta T_s}$, $B = \int_0^{\Delta T_s} e^{A_d \tau} B_d d\tau, \Delta u(k) = [\Delta P^{ref}(k), \Delta Q^{ref}(k), \Delta v(k)]^T$, $\Delta y(k) = [\Delta P(k+1), \Delta Q(k+1), \Delta V(k+1)]^T$, $A_d = \begin{bmatrix} \frac{P^0 - P_m}{2H_t(\omega^0)^2} & \frac{1}{2H_t\omega^0} & 0 \\ 0 & -\frac{1}{T_P} & 0 \\ 0 & 0 & -\frac{1}{T_Q} \end{bmatrix}$, $B_d = \begin{bmatrix} 0 & 0 & \frac{K_v}{2H_t\omega^0} \\ \frac{1}{T_P} & 0 & \frac{K_v}{T_P} \\ 0 & \frac{1}{T_Q} & 0 \end{bmatrix}, C = \begin{bmatrix} 0 & 1 & 0 \\ 0 & 0 & 1 \\ 0 & \frac{\partial V}{\partial P} & \frac{\partial V}{\partial Q} \end{bmatrix}$, ΔT_S is the sampling time.

Reactive power devices are important means of maintaining voltage stability. Especially under sandstorm weather, the synergistic action of SVG and OLTC can rapidly compensate reactive power deficits and optimize bus voltages. SVG is used to rapidly cope with the instantaneous impact brought by sandstorm weather. Considering that SVG mainly regulates voltage by controlling reactive power, the voltage-power linearized state equation of SVG with respect to the bus voltage is expressed as:

$$\Delta V_i = \frac{\partial V_i}{\partial Q_{SVG}} \Delta Q_{SVG} \tag{11}$$

where ΔV_i is the voltage increment, and ΔQ_{SVG} is the reactive power increment of SVG. The partial derivative coefficient of voltage sensitivity with respect to power is calculated as:

$$\frac{\partial V_i}{\partial Q_{SVG}} = \frac{1}{\partial V_i}\mathrm{Re}(\underline{V}_i \frac{\overline{V}_i}{\partial Q_{SVG}}) \tag{12}$$

Considering that OLTC control is on the second-level timescale, its roles in wind farm voltage control is to adjust in advance according to the prediction before the sandstorm, so as to reduce the pressure on SVG. OLTC regulates voltage by changing the tap ratio, and the sensitivity of node voltage with respect to OLTC tap changes is calculated as:

$$\frac{\partial V_i}{\partial N_{tap}} = V_{k1} \cdot \Delta V_{tap} \cdot \frac{V_{N1}}{V_{N2}} \cdot \frac{\partial V_i}{\partial V_k} \tag{13}$$

where V_{k1} is the primary voltage of the transformer, ΔV_{tap} is the voltage step size for each tap, and V_{N1}, V_{N2} is the reference voltage on both sides of transformer.

3.2. MPC-Based Wind Farm Voltage Control

MPC computes the optimal control inputs by predicting system behavior over the prediction horizon, thereby achieving closed-loop regulation. Within the prediction horizon T_P, there exists N_C control period T_C. The number of prediction steps within one control period and the total number of prediction steps are $N_S = T_C/\Delta T_P$ and $N_P = T_P/\Delta T_P$,

respectively. In the MPC framework proposed in this paper, different devices have differentiated control period settings: wind turbine converters and SVG use sampling time ΔT_P as their control time to cope with rapid voltage fluctuations, while the control cycle of OLTC is T_C and must be greater than the mechanical delay T_{mech}.

The established wind farm voltage optimization model first determines the optimal reactive power outputs of wind turbines, SVG, and OLTC to minimize the voltage deviation from the reference value:

$$Obj_1 = \sum_{i=1}^{N_C} \sum_{k=1}^{N_S} \left\| V_i(k) - V^{ref} \right\|^2 \tag{14}$$

where V^{ref} is the initial voltage value, $V_i(k)$ is the changes in OLTC taps, voltage prediction value, which can be expressed as:

$$V_i(k) = V_i(0) + \frac{\partial V_i}{\partial P_{WT}} \Delta P_{WT} + \frac{\partial V_i}{\partial Q_{WT}} \Delta Q_{WT} + \frac{\partial V_i}{\partial Q_{SVG}} \Delta Q_{SVG} + \frac{\partial V_i}{\partial N_{tap}} \Delta n_{tap}(i) \tag{15}$$

where $V_i(0)$ is the initial voltage value, $\Delta n_{tap}(i)$ is the change in OLTC tap position, $\partial V_i / \partial P_{WT}$ and $\partial V_i / \partial Q_{WT}$ are the sensitivity of voltage to wind turbines, and $\Delta P_{WT}, \Delta Q_{WT}$ are the increment of active and reactive power of the wind turbines.

Secondly, economic operation is considered by maximizing the active power output of wind turbines:

$$Obj_2 = \sum_{i=1}^{N_C} \sum_{k=1}^{N_S} \left\| P_i(k) - P^{ref} \right\|^2 \tag{16}$$

Finally, the reduction in OLTC switching operations is considered as:

$$Obj_3 = \sum_{i=1}^{N_C} \left\| n_{tap}(i) - n_{tap}(i-1) \right\|^2 \tag{17}$$

Considering the security priority at different stages of sandstorm weather, a comprehensive objective function is established to dynamically adjust according to the sandstorm weather stage:

$$J = \lambda_V Obj_1 + \lambda_P Obj_2 + \lambda_N Obj_3 \tag{18}$$

where $\lambda_V, \lambda_P, \lambda_N$ are the weighting coefficients for the voltage deviation, active power deviation, and OLTC tap adjustment objectives, respectively.

The constraints ensure the feasibility and safety of the control strategy. The wind turbine constraints include the upper and lower limits of terminal voltage, active and reactive power references, and rotor speed to prevent equipment overload or instability:

$$\begin{aligned} &V_{\min} \le V_i(k) \le V_{\max} \\ &P_{i,\min}^{ref} \le P_i^{ref}(k) \le P_{i,\max}^{ref} \\ &Q_{i,\min}^{ref} \le Q_i^{ref}(k) \le Q_{i,\max}^{ref} \\ &\omega_{\min} \le \omega_i(k) \le \omega_{\max} \end{aligned} \quad , \forall i \in (1, N_w), k \in (1, N_p) \tag{19}$$

where $V_{\min}, V_{\max}$ are the minimum and maximum terminal voltages for safe operation of the ith wind turbine, $P_{i,\min}^{ref}, P_{i,\max}^{ref}, Q_{i,\min}^{ref}, Q_{i,\max}^{ref}$ are the minimum and maximum reference values of active and reactive power for the ith wind turbine, $\omega_{\min}, \omega_{\max}$ are the minimum and maximum rotor speeds for safe operation, and N_w is the number of wind turbines.

The SVG constraints limit the reactive power output range to avoid over-compensation:

$$Q_{\min} \le Q_i \le Q_{\max} \tag{20}$$

where $Q_{\min}, Q_{\max}$ are the minimum and maximum reactive power outputs of SVG.

The OLTC constraints specify the tap step size and range to reduce mechanical stress:

$$\underline{n}_{tap} \leq n_{tap}(i) \leq \overline{n}_{tap} \tag{21}$$

$$\Delta\underline{n}_{tap} \leq \Delta n_{tap}(i) \leq \Delta\overline{n}_{tap} \tag{22}$$

where $\underline{n}_{tap}, \overline{n}_{tap}$ are the upper and lower limits of the tap position, and $\Delta\underline{n}_{tap}, \Delta\overline{n}_{tap}$ are the upper and lower limits of tap variation.

4. Two-Stage Fast Topology Reconfiguration

This section presents the minute-level topology reconfiguration method for new power systems with high wind power integration. A fast network topology reconfiguration method is proposed based on a two-stage heuristic strategy. This method can rapidly determine the optimal switch combination under radiality constraints, reducing system network losses and improving long-term operational economy under sandstorm weather.

4.1. Mathematical Description of the Reconfiguration Problem

The NR problem is a mixed-integer nonlinear optimization problem, with the objective of minimizing the total active power loss of the system, which can be expressed as the sum of the square of each branch current and its corresponding resistance:

$$\min P_{loss} = \sum_{k \in \Omega_S} |I_k|^2 R_k \tag{23}$$

Meanwhile, the optimization process must satisfy a series of strict operational constraints. On one hand, the active and reactive powers in the network must achieve global balance, and the node voltages and branch currents must be maintained within their safety limits:

$$I = Y_{pr} K A U \tag{24}$$

$$S_i^{inj} = \sum_{j \in \Omega_B} U_i U_j^* Y_{i,j}^*, \ \forall i \in \Omega_B \tag{25}$$

$$|U_i|^{min} \leq |U_i| \leq |U_i|^{max}, \ \forall i \in \Omega_B \tag{26}$$

$$|I_k| \leq |I_k|^{max}, \ \forall k \in \Omega_S \tag{27}$$

where I, U are column matrices whose elements represent the branch currents and node voltages of the network, Ω_B, Ω_S are the sets of nodes and branches in the power network, K is a diagonal matrix composed of binary switch variables, Y_{pr}, A are the original admittance matrix and incidence matrix of the network with all switches closed, S_i^{inj} is the complex power injection at the ith node, $|U_i|^{\min}$, $|U_i|^{\max}$ are the upper and lower limits of the voltage magnitude at the ith node, and $|I_k|^{\max}$ is the current magnitude limit of the kth branch.

On the other hand, the reconfigured topology must always maintain a radial structure:

$$rank(KA) = N_b - 1 \tag{28}$$

$$trace(KA) = N_b - 1 \tag{29}$$

where N_b is the number of nodes. The rank constraint ensures that all nodes remain connected after topology reconfiguration, while the trace constraint guarantees that the number of energized branches equals $N_b - 1$, thereby preventing loop formation and maintaining a radial network structure.

4.2. Two-Stage Heuristic Solution Strategy

Directly solving the above mixed-integer nonlinear model is computationally intensive for large-scale systems. Therefore, a two-stage heuristic strategy is adopted to accelerate the solution process while maintaining solution quality, adapting to the minute-level fast decision-making requirements under sandstorm weather.

The objective of Stage 1 is to rapidly generate a feasible radial topology from the fully closed network. All switches are initially closed, forming multiple loops, and a Newton–Raphson power flow is performed to obtain all branch currents. The switches are then sorted in ascending order of branch current magnitude. Each switch is sequentially attempted to be opened. If radiality is maintained, the switch is permanently opened. Otherwise, it is reclosed. This process continues until the number of closed switches equals $N_b - 1$, yielding a feasible radial network.

This strategy is based on the heuristic that branches with smaller currents contribute less to power losses and have less impact on power flow distribution. By opening low-current branches first, the risk of voltage violations or infeasible topologies is minimized. Only one power flow calculation is required to complete the initial reconfiguration, avoiding the process of recalculating power flow at each step and significantly reducing computational burden.

Stage 2 further reduces network losses through exchange of switch states based on the radial network obtained from Stage 1. The core idea is that closing a tie switch creates a unique loop, and one sectional switch on that loop must be opened to restore radiality. The number of possible exchanges grows rapidly with network size, so the bus injection to branch current (BIBC) matrix is used to efficiently identify the set of switches on each loop. For a tie switch connecting two specific nodes, the switches on the resulting loop are identified by comparing the branch current sensitivities to the injections at those two nodes.

Once the loop switches are identified, Kirchhoff's current law is applied to derive approximate update formulas for each branch current after the exchange, without requiring a full power flow recalculation. Based on these estimated currents, the loss variation caused by each candidate exchange is rapidly calculated. The switch pair yielding the greatest loss reduction is selected for execution, followed by a power flow calculation to verify constraint satisfaction. If all constraints are satisfied, the network state is updated and the next round of exchange continues; otherwise, the iteration terminates and the final topology is output.

The two-stage strategy requires only one full power flow calculation in Stage 1 and one verification per accepted exchange in Stage 2, while all other evaluations are based on simple algebraic calculations. Therefore, the proposed method achieves high computational efficiency and is highly suitable for minute-level online reconfiguration scenarios. Through information exchange with the second-level MPC controller, the minute-level reconfiguration adjusts the network topology according to the latest operating conditions, thereby continuously improving system economy while maintaining voltage stability.

5. Case Study

The proposed strategy is validated on a 33-node power distribution network integrated with a wind farm equipped with SVG and OLTC. The configuration of the test system is shown in Figure 2. The initial switch configuration of the test system consists of switches 1–32 in the closed state and switches 33–37 in the open state, with the wind farm connected at node 26. The simulations are conducted in MATLAB R2019a on a computer equipped with an Intel Core i7-12700F 2.10 GHz CPU and 32-GB RAM. To ensure the reproducibility of the proposed multi-timescale cooperative voltage control method, the main parameters of the wind turbines, SVG, OLTC, MPC controller, and topology reconfiguration strategy

are summarized in Table 1. Since the proposed MPC controller adopts different control priorities during different sandstorm evolution stages, the corresponding objective function weighting factors are further provided in Table 2.

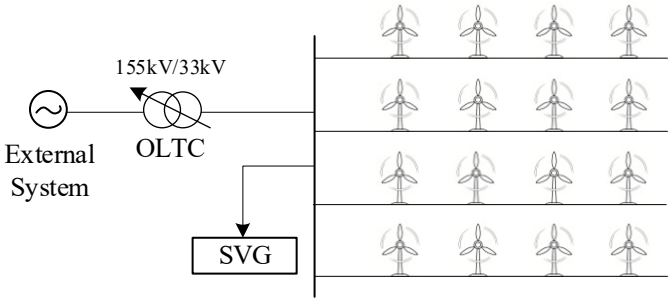


Figure 2. Topology of the wind farm.

Table 1. Main parameters used in the simulation.

Category	Parameter	Value
Wind turbine	Number	16
	Rated capacity	2.5 MW
SVG	Reactive power capacity	−22 Mvar ~ +22 Mvar
OLTC	Tap range	−8 to +8
MPC controller	Sampling interval	1 s
	Prediction horizon	10 s
Topology reconfiguration	Reconfiguration interval	30 min

Table 2. Weighting factors of MPC objective function.

Sandstorm Stage	λ_V	λ_P	λ_N
Initial stage	0.4	0.5	0.6
Rising stage	0.4	0.3	0.25
Peak stage	0.2	0.2	0.15

To represent the wind disturbance caused by the sandstorm, a composite engineering wind-field model is adopted. The effective wind speed at each wind turbine is determined by four components: the time-varying mean wind speed, wind shear, turbulence, and wake effects. The sandstorm process is divided into four stages, namely the initial normal stage, rising stage, peak stage, and attenuation stage. The mean wind speed is varied gradually between these stages to describe the temporal evolution of the sandstorm.

During the peak stage, the mean wind speed is set to 16 m/s to represent the high-wind condition, while the turbulence intensity of 0.2 is used to describe strong short-term wind fluctuations. The wind-shear component is described by the power-law model, with a wind-shear exponent of 0.14, consistent with the engineering wind conditions considered in IEC 61400-1 [23]. The turbulence component is generated based on the Kaimal spectrum specified in IEC 61400-1. The wake effect is represented using the Jensen engineering wake model [24]. The resulting wind-speed components are combined to obtain the effective wind speed at each wind turbine, which is then used as the external wind-speed input to the nonlinear variable-speed wind-turbine model.

As shown in Figure 3, the instantaneous wind speed can reach approximately 35–40 m/s during the severe stage of the sandstorm. These values are caused by stochastic turbulence fluctuations imposed on the mean wind speed and should not be interpreted as sustained mean wind speeds. Therefore, the wind-speed profile is intended to represent a severe and rapidly varying wind disturbance for evaluating the proposed voltage-

control method, rather than to reproduce the wind conditions of one specific measured sandstorm event.

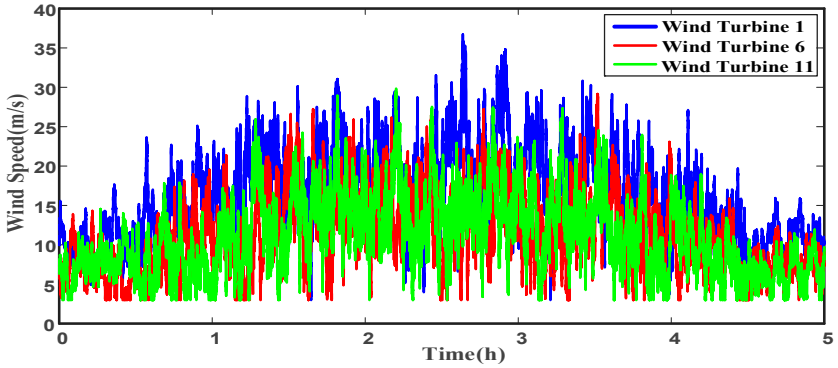


Figure 3. Wind speed curves of wind turbines in the wind farm during the sandstorm event.

It should be noted that the detailed cut-out protection of the wind turbines is not explicitly modeled in this study. In particular, the protection threshold, protection delay, shutdown process, reconnection condition, and restart process are not included in the present simulation model. Therefore, when an instantaneous wind-speed sample exceeds a conventional cut-out threshold, it is not directly treated as an immediate turbine shutdown event.

This treatment is related to the purpose of the present study. The proposed method is designed to evaluate multi-timescale cooperative voltage control under severe and rapidly varying sandstorm wind disturbances. The wind-speed profile is therefore used as a prescribed external disturbance for the wind-turbine dynamic model. The instantaneous wind-speed values of 35–40 m/s in Figure 3 are short-duration turbulence fluctuations rather than sustained wind conditions at this level.

The wind-speed signal is applied to the nonlinear variable-speed wind-turbine model, and the active-power response is obtained from the dynamic turbine model. Therefore, the active-power results presented in this study describe the dynamic response of the modeled wind turbines to the prescribed wind disturbance. They should not be interpreted as the actual active-power response of a physical wind turbine after cut-out protection has been activated. Similarly, the voltage-control results represent the response of the proposed control method under the specified wind disturbance and the corresponding dynamic active- and reactive-power responses of the modeled wind turbines. They do not represent the voltage response after physical turbine disconnection caused by cut-out protection. If cut-out protection were explicitly included, turbine shutdown would change the active and reactive power balance of the distribution network and could consequently affect the voltage-control results.

A complete representation of this process would require additional models for the cut-out threshold, protection delay, turbine shutdown, reconnection, and restart dynamics. These protection-related dynamics are outside the main scope of the present study. The corresponding limitation is stated here to clarify the interpretation of the simulation results.

On the second-level timescale, the proposed MPC-based multi-device cooperative optimization strategy is evaluated. Figure 4 shows the total active power output of the wind farm during the sandstorm. Although the wind speed increases significantly during the sandstorm event, the active power output of the wind farm remains slightly below 1 p.u. due to practical operating constraints and safety margins of wind turbine systems. This limitation ensures reliable operation while maintaining sufficient reactive power support capability for voltage regulation. The output increases sharply during the ramp-up stage and remains high during the peak stage, and gradually decreases as the disturbance sub-

sides. This result indicates that wind energy resources have higher short-term availability under extreme weather conditions, but also imposes greater pressure on grid connection point voltage control, raising higher requirements for wind farm reactive power support capability and multi-device coordinated control capability.

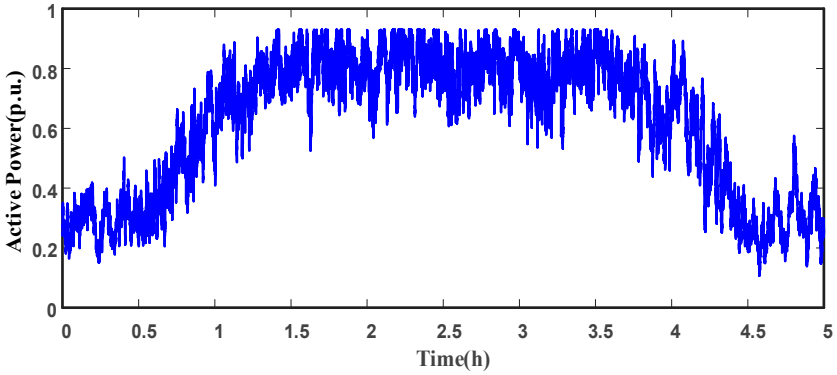


Figure 4. Total active power output of the wind farm.

Figure 5 compares the grid connection point voltage under the proposed MPC and traditional droop control. Traditional droop control is selected as the benchmark because it is a widely adopted voltage regulation strategy in practical power systems due to its simple structure and fast response capability. However, droop control mainly relies on local voltage deviations and lacks prediction capability and coordinated optimization among multiple regulation devices. In contrast, the proposed MPC method considers future system states and coordinates wind turbine converters, SVG, and OLTC, enabling more effective voltage regulation under rapidly varying wind speed conditions. As shown in Figure 5, both methods maintain the voltage within the allowable range, but the MPC provides a smoother response with smaller deviations. Compared with droop control, MPC significantly reduces voltage deviations and fluctuation amplitudes during sandstorm disturbances, demonstrating superior dynamic voltage support performance.

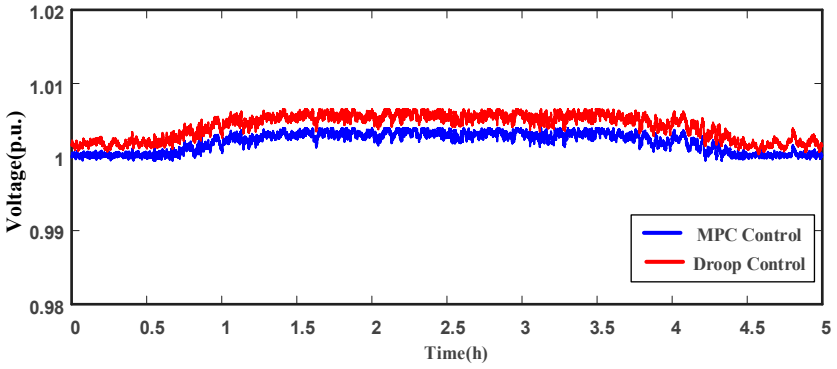


Figure 5. Comparison of grid connection point voltage control performance.

Figures 6 and 7 show the reactive power outputs of wind turbines and SVG. Under droop control, the reactive power outputs of wind turbines and SVG are generally lower than those under the MPC strategy. This is because droop control performs passive regulation based on local voltage deviations. In contrast, MPC actively regulates reactive power through rolling optimization, thereby improving voltage control effectiveness. Figure 6 shows that the total reactive power output of wind turbines maintains continuous variation throughout the disturbance process, indicating that the wind turbines can provide certain reactive power support, undertaking part of the fundamental regulation tasks. Figure 7 shows that SVG variations are more pronounced, indicating that SVG remains the primary

dynamic reactive power regulation device under rapid voltage disturbances. The synergistic effect of the two devices ensures that the total reactive power output of the wind farm possesses both sufficient regulation capability and good smoothness.

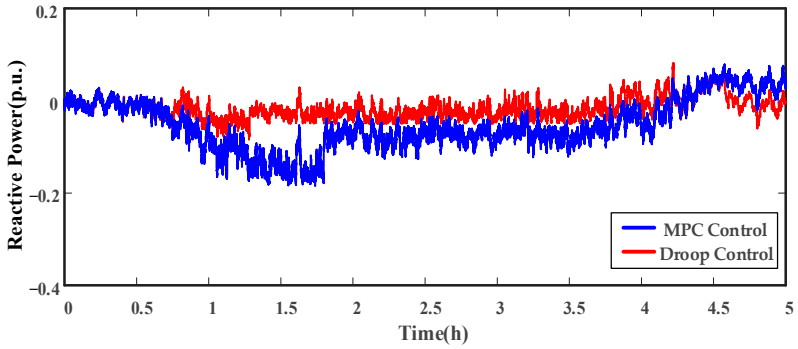


Figure 6. Total reactive power output of wind turbines.

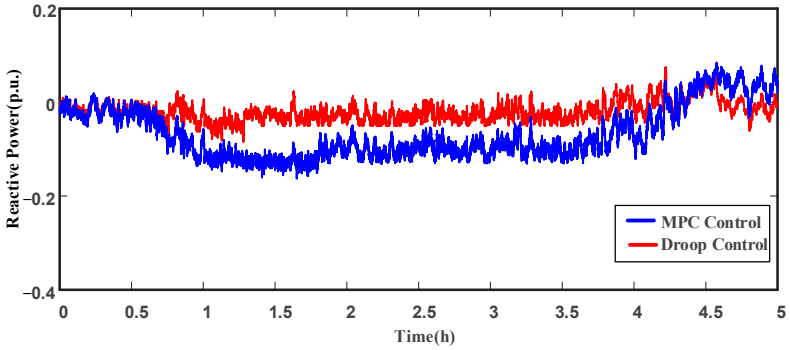


Figure 7. Dynamic reactive power output of SVG.

Figure 8 shows the OLTC tap adjustments. Under the proposed MPC, OLTC operations are significantly fewer than under droop control, with much less frequent switching actions. This indicates that under MPC coordinated control, fast voltage deviations are mainly compensated by the wind turbine and SVG on the short timescale, while OLTC primarily undertakes steady-state voltage setting tasks on the slow timescale.

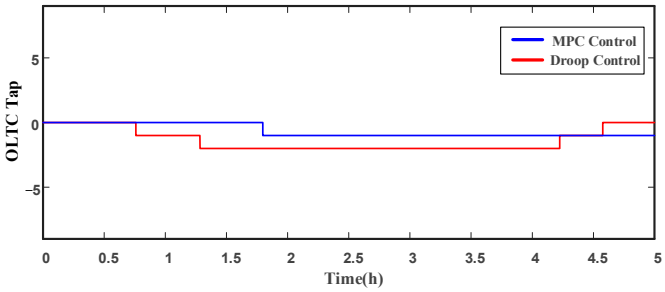


Figure 8. OLTC tap adjustment curve.

On the minute-level timescale, the proposed efficient two-stage heuristic method for power network topology reconfiguration is evaluated, with the objective of minimizing total system active power losses under radiality constraints. This strategy not only significantly shortens the computation cycle but also effectively improves the efficiency of the optimization process. Table 3 presents the detailed results of implementing this strategy every 30 min for power network switch planning.

Table 3. Two-stage reconfiguration results.

Time	Open Switch Nos.	Time	Open Switch Nos.
0:00–0:30	7, 11, 14, 28, 31	2:30–3:00	7, 8, 14, 28, 31
0:30–1:00	7, 11, 14, 28, 31	3:00–3:30	7, 8, 14, 28, 31
1:00–1:30	7, 11, 14, 28, 31	3:30–4:00	7, 9, 14, 28, 32
1:30–2:00	7, 11, 14, 28, 31	4:00–4:30	7, 9, 14, 28, 32
2:00–2:30	7, 8, 14, 28, 31	4:30–5:00	7, 9, 14, 28, 32

Table 4 compares the proposed two-stage heuristic method with MP at the 5th hour. MP is selected as the benchmark because it is a representative optimization-based method for network reconfiguration and can obtain high-quality solutions by directly solving the mathematical model. However, the mixed-integer nonlinear characteristics of the reconfiguration problem lead to increased computational burden, which limits its application in online scenarios. Both methods achieve the same loss of 28.334 kW, but the proposed method requires only 0.066 s compared with 1.2 s for MP, highlighting the computational efficiency advantage of the proposed two-stage heuristic algorithm. Therefore, the proposed method provides a more practical solution for minute-level online network optimization under sandstorm weather conditions.

Table 4. Comparison of two reconfiguration methods.

Method	Loss (kW)	Time (h)	Open Switch Nos.
MP	28.334	1.2	7, 9, 14, 28, 32
Proposed Method	28.334	0.066	7, 9, 14, 28, 32

Although more advanced learning-based or intelligent optimization methods have been reported for voltage control and network reconfiguration, this study focuses on developing an online applicable control framework under extreme weather conditions. Therefore, practical benchmark methods with strong engineering relevance are selected to evaluate the voltage regulation capability and computational efficiency of the proposed framework.

6. Conclusions

This paper proposes a multi-timescale cooperative voltage control method for new power systems under sandstorm weather conditions, which effectively addresses the challenges of transient voltage fluctuations caused by rapid wind speed variations and long-term operational economy. A second-level and minute-level coordinated control framework is developed to achieve the cooperation between fast reactive power regulation and topology optimization. By integrating wind turbine converters, SVG, OLTC, and network switches, the proposed strategy enhances the dynamic reactive power support capability of new power systems under extreme weather conditions.

Simulation results demonstrate the effectiveness of the proposed coordinated optimization strategy. The proposed MPC-based voltage control method utilizes prediction and coordinated optimization to effectively suppress voltage fluctuations, avoiding the voltage fluctuations and delayed response caused by passive droop control. The grid connection point voltage can be maintained within a stable range from 1.000 p.u. to 1.003 p.u. with a smoother response. At the minute-level timescale, the proposed two-stage heuristic topology reconfiguration method rapidly determines optimal switch configurations during each optimization period and effectively reduces total network losses. The results verify that the proposed strategy can simultaneously improve transient stability and long-term operational economy under extreme weather conditions, providing a practical solution for

new power systems with high renewable energy penetration. Future work will focus on extending the proposed framework to different network structures and more complex extreme weather scenarios, as well as incorporating the detailed cut-out protection dynamics of wind turbines to enhance practical applicability.

Author Contributions: Conceptualization, Q.Z. and H.Z.; methodology, L.L.; software, J.W.; validation, X.C. and Y.L.; formal analysis, Q.Z.; investigation, Q.Z.; resources, J.Z.; data curation, J.W.; writing—original draft preparation, L.L.; writing—review and editing, L.L.; visualization, Q.Z.; supervision, J.W.; project administration, H.Z.; funding acquisition, X.C. All authors have read and agreed to the published version of the manuscript.

Funding: This research was funded by the State Grid Shanxi Electric Power Company Technology Project [52053025000X].

Data Availability Statement: The data presented in this study are available upon request from the corresponding author due to confidentiality reasons.

Conflicts of Interest: Author Qian Zhang, Huiping Zheng, Xueting Cheng was employed by the company State Grid Shanxi Electric Power Research Institute. The remaining authors declare that the research was conducted in the absence of any commercial or financial relationships that could be construed as a potential conflict of interest.

Abbreviations

The following abbreviations are used in this manuscript:

MPC	Model Predictive Control
SVG	Static Var Generator
OLTC	On-Load Tap Changer
ADMM	Alternating Direction Method of Multipliers
NR	Network Reconfiguration
MP	Mathematical Programming
MILP	Mixed-Integer Linear Programming
MISOCP	Mixed-Integer Second-Order Cone Programming

References

1. Xu, D.; Li, H.; Yang, X.; Yang, H.; Yang, H.; Bai, Z. Cooperative operation of P2G-based multi-energy systems considering proactive demand response of energy-intensive multi-process industrial loads. *IEEE Trans. Ind. Appl.* **2025**, 1–13. [CrossRef]
2. Wang, Y.; Qiu, D.; Wang, Y.; Sun, M.; Strbac, G. Graph learning-based voltage regulation in distribution networks with multi-microgrids. *IEEE Trans. Power Syst.* **2024**, *39*, 1881–1895. [CrossRef]
3. Xu, C.; Cui, S.; Wei, L.; Zhu, B.; Ai, X.; Fang, J.; Wen, J. Wind power forecasting under extreme weather: A novel few-shot learning architecture. *IEEE Trans. Sustain. Energy* **2026**, *17*, 788–803. [CrossRef]
4. Guo, X.; Hu, Z.; Wang, S.; Reyna, M.; Yao, N.; Li, T.; Zhou, W. A multi-layer coordinated reactive power optimization method for a distribution network considering large-scale distributed wind-photovoltaic hierarchical access. *Power Syst. Prot. Control* **2024**, *52*, 113–122. [CrossRef]
5. Nguyen, H.M.; Torres, J.L.R.; Lekić, A.; Pham, H.V. MPC based centralized voltage and reactive power control for active distribution networks. *IEEE Trans. Energy Convers.* **2021**, *36*, 1537–1547. [CrossRef]
6. Maharjan, S.; Khambadkone, A.M.; Peng, J.C.-H. Robust constrained model predictive voltage control in active distribution networks. *IEEE Trans. Sustain. Energy* **2021**, *12*, 400–411. [CrossRef]
7. Wang, Y.; Xu, Y.; Tang, Y.; Syed, M.H.; Guillo-Sansano, E.; Burt, G.M. Decentralised-distributed hybrid voltage regulation of power distribution networks based on power inverters. *IET Gener. Transm. Distrib.* **2019**, *13*, 444–451. [CrossRef]
8. Šulc, P.; Backhaus, S.; Chertkov, M. Optimal distributed control of reactive power via the alternating direction method of multipliers. *IEEE Trans. Energy Convers.* **2014**, *29*, 968–977. [CrossRef]
9. Jiao, W.; Chen, J.; Wu, Q.; Li, C.; Zhou, B.; Huang, S. Distributed coordinated voltage control for distribution networks with DG and OLTC based on MPC and gradient projection. *IEEE Trans. Power Syst.* **2022**, *37*, 680–690. [CrossRef]

10. Qin, W.; Moroshko, E.; Kiprakis, A. Integrated resilience optimization for distribution networks under extreme weather: Joint dynamic reconfiguration and mobile energy storage dispatch. In Proceedings of the 2026 IEEE Power & Energy Society International Meeting (PESIM), Hong Kong, China, 1–5 January 2026.
11. Gao, Y.; Wang, W.; Shi, J.; Yu, N. Batch-constrained reinforcement learning for dynamic distribution network reconfiguration. *IEEE Trans. Smart Grid* **2020**, *11*, 5357–5369. [CrossRef]
12. Ma, W.; Gao, H.; Yang, Y.; Wang, C.; Pan, H.; Liu, Y.; Liu, J. Two-stage optimal operation for distribution network based on fast identification of reconfiguration level. *Proc. CSEE* **2022**, *42*, 5154–5168. [CrossRef]
13. Lei, C.; Bu, S.; Wang, Q.; Liang, L. Observability defense-constrained distribution network reconfiguration for cyber-physical security enhancement. *IEEE Trans. Smart Grid* **2024**, *15*, 2379–2382. [CrossRef]
14. Wang, Y.; Xu, Y.; Li, J.; He, J.; Wang, X. On the radiality constraints for distribution system restoration and reconfiguration problems. *IEEE Trans. Power Syst.* **2020**, *35*, 3294–3296. [CrossRef]
15. Liu, Z.; Liu, Y.; Qu, G.; Wang, X.; Wang, X. Intra-day dynamic network reconfiguration based on probability analysis considering the deployment of remote control switches. *IEEE Access* **2019**, *7*, 145272–145281. [CrossRef]
16. Wang, S.; Wei, J.; Huang, S.; Liu, L.; Cheng, X.; Peng, H. Real-time multi-time-scale voltage control and reconfiguration for renewable power system with gradient projection and switch exchange method. *Electr. Power Syst. Res.* **2026**, *250*, 112173. [CrossRef]
17. Huang, D.; Yu, J.; Cui, C.; Dong, Q.; Zhou, Y.; Gong, C. Voltage optimization for PV-ES distribution network with multi-timescale deep reinforcement learning method. *Proc. CSEE* **2025**, *45*, 6709–6723. [CrossRef]
18. Zhang, T.; Yu, L.; Yue, D.; Dou, C.; Xie, X.; Hancke, G.P. Two-timescale coordinated voltage regulation for high renewable-penetrated active distribution networks considering hybrid devices. *IEEE Trans. Ind. Inform.* **2024**, *20*, 3456–3467. [CrossRef]
19. Wei, L.; Wei, J.; Huang, S.; Li, C.; Zhu, L.; Chen, K.; Wang, S.; Wang, L. Hierarchical optimal continuous fault ride-through control scheme for heterogeneous wind farm with grid-forming and grid-following wind turbines. *IEEE Trans. Sustain. Energy* **2026**, *17*, 2233–2248. [CrossRef]
20. Guo, Y.; Wu, Q.; Gao, H.; Huang, S.; Zhou, B.; Li, C. Double-time-scale coordinated voltage control in active distribution networks based on MPC. *IEEE Trans. Sustain. Energy* **2020**, *11*, 294–303. [CrossRef]
21. Dar, M.R.; Ganguly, S. A distributionally robust chance constrained model predictive control based coordinated voltage control of active distribution networks with uncertainties under high photovoltaic penetration. *IEEE Trans. Ind. Appl.* **2026**, *62*, 5160–5171. [CrossRef]
22. Yang, Q.; Wang, G.; Sadeghi, A.; Giannakis, G.B.; Sun, J. Two-timescale voltage control in distribution grids using deep reinforcement learning. *IEEE Trans. Smart Grid* **2020**, *11*, 2313–2323. [CrossRef]
23. *IEC 61400-1:2019*; Wind Energy Generation Systems—Part 1: Design Requirements. IEC: Geneva, Switzerland, 2019.
24. Jensen, N.O. *A Note on Wind Generator Interaction*; Risø-M No. 2411; Risø National Laboratory: Roskilde, Denmark, 1983.

Disclaimer/Publisher's Note: The statements, opinions and data contained in all publications are solely those of the individual author(s) and contributor(s) and not of MDPI and/or the editor(s). MDPI and/or the editor(s) disclaim responsibility for any injury to people or property resulting from any ideas, methods, instructions or products referred to in the content.